



A colorimetric immunoassay for the detection of human vascular endothelial growth factor 165 (VEGF₁₆₅) based on anti-VEGF-iron oxide nanoparticle conjugation

Hülya Kuduğ Ceylan¹ · Fatma Öztürk Kırbay² · İdris Yazgan³ · Murat Elibol⁴

Received: 14 September 2023 / Accepted: 22 January 2024 / Published online: 14 February 2024
© The Author(s) 2024

Abstract

Vascular endothelial growth factor (VEGF) is an indispensable element in many physiological processes, while alterations in its level in the circulating system are signs of pathology-associated diseases. Therefore, its precise and selective detection is critical for clinical applications to monitor the progression of the pathology. In this study, an optical immunoassay biosensor was developed as a model study for detecting recombinant VEGF₁₆₅. The VEGF₁₆₅ sample was purified from recombinant *Kluyveromyces lactis* GG799 yeast cells. Indirect ELISA was used during the detection, wherein iron oxide nanoparticles (FeNPs) were utilized to obtain optical signals. The FeNPs were synthesized in the presence of lactose p-amino benzoic acid (LpAB). VEGF₁₆₅ antibody was conjugated to the LpAB-FeNPs through EDC/NHS chemistry to convert the iron oxide nanoparticles into VEGF₁₆₅ specific probes. The specificity of the prepared system was tested in the presence of potential serum-based interferents (i.e., glucose, urea, insulin, C-reactive protein, and serum amyloid A), and validation studies were performed in a simulated serum sample. The proposed immunoassay showed a wide detection range (0.5 to 100 ng/mL) with a detection limit of 0.29 ng/mL. These results show that the developed assay could offer a sensitive, simple, specific, reliable, and high-throughput detection platform that can be used in the clinical diagnostics of VEGF.

Keywords Human vascular endothelial growth factor · Iron oxide nanoparticle · Immunoassay · Indirect ELISA · Optical detection

Hülya Kuduğ Ceylan contributed to this study at Ege University, Bioengineering Department, 35100, Bornova, Izmir, Turkey.

✉ Hülya Kuduğ Ceylan
hulya.kudug@gop.edu.tr

✉ Fatma Öztürk Kırbay
ffatma.ozturkk@gmail.com

¹ Department of Basic Pharmaceutical Sciences, Faculty of Pharmacy, Tokat Gaziosmanpaşa University, 60250 Tokat, Turkey

² Biochemistry Department, Faculty of Science, Ege University, Bornova, 35100 Izmir, Turkey

³ Center for Biosensors and Material Science, Department of Biology, Faculty of Science and Art, Kastamonu University, 37100 Kastamonu, Turkey

⁴ Bioengineering Department, Ege University, Bornova, 35100 Izmir, Turkey

Introduction

Vascular endothelial growth factor (VEGF) is one of the most important cytokines that plays an essential role in vascular development and permeability [1]. VEGF and its receptors have been considered fundamental regulators for angiogenesis and vasculogenesis, which describe the processes of new capillary blood vessel formation [2]. VEGF triggers new blood vessel formation through the induction of vascular endothelial cells that can proliferate, migrate, and differentiate in healthy tissues [3, 4].

VEGF₁₆₅ is the most dominant isoform of the human VEGF (also called VEGF-A) family and has the highest biological activity during angiogenesis [5]. Particularly, it participates in a variety of physiological angiogenic processes, including wound healing [6], female reproduction cycle [7], embryogenesis [8], neural development [9], bone formation [10], and hematopoiesis [11] in healthy adults. However, under certain circumstances, the overexpression of VEGF is well correlated with rheumatoid arthritis

[12], Parkinson's disease [13], psoriasis [14], and several ocular diseases [15, 16], while VEGF activity continues physiologically normal during vascular development. Besides, VEGF has also been widely described as a major tumor angiogenic factor in many tumor types [17, 18]. Particularly, VEGF participates in different stages of tumor, including development, progression, and metastasis, which can also orchestrate tumorigenic angiogenesis in ovarian [19], pancreatic cancer [20], lung (e.g., non-small cell lung cancer) [21], breast [22], oral [23], colorectal cancer [24], and liver cancers [25]. In this regard, elevated VEGF levels have been proposed as an essential biomarker in many types of cancers. In addition to cancer, such diseases as age-related macular degeneration in the eyes result in increased VEGF concentration in patients' eyes. Therefore, the detection of the VEGF concentration in the patient's retina is critical for the determination of the amount of anti-VEGF drug for intravitreal injections [26, 27].

Due to the critical importance of VEGF in biomedical research, early diagnosis, and medical applications, the detection and quantification of VEGF is strongly required to trace its levels in biological samples. Until now, a variety of approaches for the detection of VEGF have been reported, including enzyme-linked immunosorbent assay (ELISA) [28] (the standard assay format), fluorescence in situ hybridization (FISH) [29], immunohistochemistry (IHC) [30], and fluorescent spectrometry [31–33]. Even though each of these techniques has such superiorities, there is no available technique to overcome such drawbacks, including excessive time requirement, expensiveness, and requirements of complicated instrumentation. Among the analytical approaches in biosensor development, colorimetric techniques can overcome these shortcomings, which are commonly used for field analysis and point-of-care diagnosis for many applications. In the case of antibody-antigen-based reactions, antigen–antibody interaction causes alteration in the color intensity with favorable properties that can fulfill the desired requirements expected from a biosensor [32–34]. In recent years, colorimetry based on metal nanoparticles has garnered significant attention and has injected fresh vigor into traditional colorimetric methods, enabling precise and accurate analyzes [35]. Among the metal-based nanoparticles, iron oxide nanoparticles (FeNPs) provide colorimetric changes with many advantages as accuracy, simplicity, broad applicability, and high selectivity, which make them appealing for straightforward colorimetric detection. In addition, FeNPs are cost-effective compared to other metals and do not cause unstable and spontaneous aggregation when they are used as probes in detections [36, 37].

In this study, the synthesized FeNPs were conjugated with VEGF₁₆₅ antibody for the colorimetric detection of VEGF₁₆₅. The sensor gave a linear range between 0.5 and 100 ng/mL with 0.29 ng/mL as the limit of detection (LOD),

which indicates that the developed immunoassay platform is highly promising for clinical applications. Furthermore, the sensing system gave excellent specificity for the potential interferents such as glucose, urea, insulin, C-reactive protein, and serum amyloid A in human serum.

Materials and methods

Reagents and strains

Recombinant *Kluyveromyces lactis* GG799 (New England Biolabs, Massachusetts, USA) was prepared by cloning the human VEGF₁₆₅ cDNA (GenBank accession no. AF486837.1) in *Xho*I and *Eco*RI sites of the pKLAC2 vector under the control of the LAC4 promoter of the reported study [38]. The recombinant strain was cultured in YCB plates (3% 1 M Tris–HCl pH 7.4, 1.17% YCB, and 2% agar) containing 5 mM acetamide and maintained at – 80 °C as glycerol stock. In addition, the expression was performed using an unoptimized YPGal medium (1% yeast extract, 2% peptone, and 4% galactose). Ni–NTA agarose resin, 1000 kDa MWCO cellulose acetate dialysis membrane, and Pierce™ BCA Protein Assay Kit were purchased from Qiagen (Hilden, Germany), Spectrum Laboratories (California, USA), and Thermo Fisher Scientific (Waltham, MA, USA), respectively. N'-Ethylcarbodiimide hydrochloride (EDC) and N-hydroxysuccinimide (NHS) were purchased from Sigma-Aldrich (St. Louis, MO, USA) while C-reactive protein (CRP) (1 mg/mL) was obtained from Prospect. Serum amyloid A (SAA) (5.6 mg/mL) was purchased from Merck (Merck Millipore, Darmstadt, Germany). The washing buffer for ELISA was 0.1 M PBS (pH 7.2) containing 0.05% Tween 20 and 0.15 M NaCl. The coating buffer for ELISA was a 50 mM carbonate buffer, pH 9.6. ELISA maxisorp immunoplate (96 flat-bottom wells) was purchased from Nunc (Roskilde, Denmark). Artificial serum sample was prepared using KCl 0.335 g/L, MgCl₂ 0.152 g/L, CaCl₂ 0.505 g/L, NaCl 8.470 g/L, NH₂CONH₂ 0.150 g/L, D-glucose 0.450 g/L, and BSA 1.000 g/L as depicted in the literature [39].

Expression and purification of recombinant human VEGF₁₆₅

The inoculum was prepared by inoculating a single colony of recombinant *K. lactis* GG799 strain in 25 mL YPGal medium and incubated at 30 °C at 250 rpm for 72 h. The culture was inoculated with a ratio of 1 to 100 in a 2 L Erlenmeyer shake flask including 300 mL YPGal, which was then followed by, and then, the expression of VEGF₁₆₅ was performed. After 48 h incubation, the culture suspension was centrifuged at 5000 rpm for 5 min at room temperature. The

supernatant containing the secreted recombinant VEGF₁₆₅ was utilized to purify the protein to use a standard protein for ELISA studies. During the purification process, the supernatant was precipitated with 60% ammonium sulfate solution in an ice bath for 60 min and then centrifuged at 12,000 rpm for 20 min. One hundred millimolars of phosphate buffer (pH 7.4) was used to dissolve the obtained protein pellet. After adding Ni–NTA agarose resin to the polycarbonate column to perform affinity-based purification chromatography, the column was washed with a 100 mM phosphate buffer (pH 7.4). The protein solution was applied to the column, and the target protein bound to the column was obtained through fractionations using the same phosphate buffer containing 300 mM imidazole. The recombinant VEGF₁₆₅ elution solution was dialyzed using 1000 kDa MWCO cellulose acetate dialysis membrane against HEPES buffer (20 mM pH 7.4) overnight + 4 °C on a magnetic stirrer. The concentration of VEGF₁₆₅ was calculated using the “Pierce™ BCA Protein Assay Kit.”

Synthesis and characterization of LpAB-FeNP

Synthesis of iron oxide nanoparticles was performed using a modified version of the reported studies [40, 41]. Briefly, 1 M citric acid was mixed with 100 mM of FeCl₃, 50 mM of FeSO₄, and 10 mM lactose p-aminobenzoic acid (the sugar ligand was provided by Dr. İdris Yazgan of Kastamonu University, Turkey). The mixture was then vortexed at 1200 rpm, and 1 M of NaOH was added to the mixture while vortexing at 600 rpm. The addition of NaOH resulted in the formation of heat, which played a vital role during the iron oxide nanoparticle formation. The colloidal nanoparticles were then transferred to a new sterile 15-mL centrifuge tube. The goal of the addition of the sugar ligand (the synthesis approach can be found elsewhere [42]) was to enhance the stability of the synthesized iron oxide nanoparticles [43] and introduce an amine group. UV–vis spectroscopy, high-resolution transmission electron microscopy-selected area diffraction (HRTEM-SAED), scanning electron microscopy (SEM), and X-ray photoelectron spectroscopy (XPS) were used to characterize LpAB-FeNPs.

Conjugation of anti-VEGF with LpAB-FeNP

Anti-VEGF conjugation to LpAB-FeNP was performed using the EDC/NHS chemistry method [44]. Anti-VEGF was activated using 50.0 mM EDC and 12.5 mM NHS and then introduced to LpAB-FeNP solution. Anti-VEGF:EDC:NHS (1:2:2; v:v:v) was mixed in PBS and incubated at 250 rpm in an orbital shaker for 15 min. After that, the LpAB-FeNP/anti-VEGF conjugate was washed three times with PBS buffer using 50-kDa centrifugal filters at 4000 rpm. Dynamic light scattering technique (DLS, Malvern Zetasizer Nano

ZS model) was used to measure the size distributions and zeta potential of LpAB-FeNP and LpAB-FeNP/anti-VEGF.

Construction of the immunoassay platform

First, the purified recombinant VEGF₁₆₅ (1 mg/mL) was diluted to 10 different concentrations (0.5, 1.0, 5.0, 10, 25, 50, 100, and 250 ng/mL) with coating buffer and added onto the ELISA plate. This plate was then incubated overnight at 4 °C. After that, unbound VEGF₁₆₅ was removed from the plate by cleaning it with a washing buffer. Next, 2 mg/mL BSA was added to each well and incubated for 1 h at room temperature as a blocking step. The conjugate of LpAB-FeNP/anti-VEGF was introduced to the plate and incubated for 1 h. After the incubation, a washing buffer was used to remove the unreacted components. The UV–Vis absorbance of this system was measured, and the absorbance varied according to the VEGF₁₆₅ concentration. The proposed immunoassay platform was similar to a previous study [45].

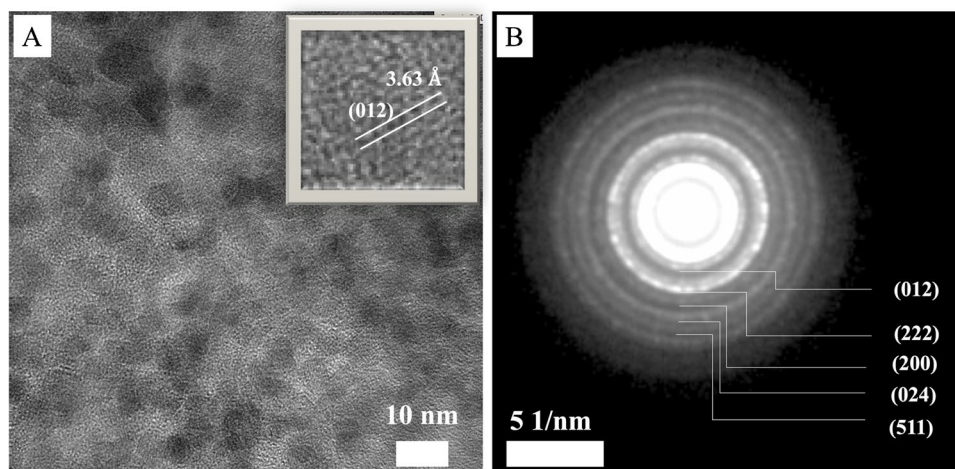
Results and discussion

Characterization of LpAB-FeNP and LpAB-FeNP/anti-VEGF

UV–vis spectroscopy played a significant role in the synthesizing of FeNP, LpAB-FeNP, and its conjugation with anti-VEGF. Fig. S1 shows absorbance at 370 nm due to the metallic iron oxide core. Fig. S2A shows the absorbance at 370 nm due to a metallic iron oxide core that confirms the presence of LpAB-FeNP [46]. The decrease in the absorbance intensity after the conjugation process indicates the successful attachment of anti-VEGF to LpAB-FeNP [47, 48]. In this study, the morphology of LpAB-FeNP and LpAB-FeNP/anti-VEGF was observed by scanning electron microscopy (SEM), as depicted in Fig. S2B and Fig. S2C. As shown in Fig. 1, the LpAB-FeNP nanoparticles exhibited a globular shape. However, after the conjugation of anti-VEGF, the morphology tended to form agglomerations and appeared as cloudy clusters. This change in morphology provides evidence of the attachment of anti-VEGF to LpAB-FeNP.

The HRTEM characterization reveals that the core size of FeNPs is in 5.5 ± 1.5 nm, where ~ 5 nm spherical ones were in the most abundant form. Selected area diffraction (SAED) patterns reveal that the FeNPs had (012), (222), (200), (024), and (511) *hkl* indices. The *hkl* (012) and (024) belong to α -Fe₂O₃, the *hkl* (200) belongs to FeO (wustite), and (222) and (511) *hkl* indices belong to Fe₃O₄ (magnetite) iron oxide crystal structures [49]. Besides, the d-spacing measured on an individual FeNP (the inset in Fig. 1A) shows that the FeNP had α -Fe₂O₃ form.

Fig. 1 **A** HRTEM and **B** SAED images of LpAB-FeNP



Zeta potential and size distribution of LpAB-FeNP and LpAB-FeNP/anti-VEGF were characterized by DLS. The average size of the LpAB-FeNP was measured to be approximately 33.9 nm, with negative zeta potential -10.1 ± 2.11 . DLS recognizes hydrodynamic size while TEM only recognizes size of the metallic core, so the size difference between the two techniques is expected. After the conjugation, the size of LpAB-FeNP/anti-VEGF increased to 74.4 nm, with a zeta potential of -13.2 ± 2.01 . The increase in hydrodynamic particle size and the difference in zeta potential confirmed the successful covalent modification.

X-ray photoelectron spectroscopy (XPS) measurements are highly accurate and provide precise details about the chemical composition of the target species. In this study, XPS was used to thoroughly examine the binding between the conjugated molecules. Therefore, LpAB-FeNP samples and LpAB-FeNP/anti-VEGF conjugates were studied using XPS (Fig. 2). Figure 2A and Fig. 2D show Fig. 2C 1 s photoelectron spectra of LpAB-FeNP and LpAB-FeNP/anti-VEGF, respectively. Figure 2A shows three main peaks of C 1 s in LpAB-FeNP spectrum. The components centered at 285.18 eV for C, 286.68 eV for C-N/C-O or C=O, and 288.38 eV for O-C=O resulted from the presence of carboxylic acid of the sugar ligand. The C 1 s spectrum for the LpAB-FeNP/anti-VEGF surface was deconvoluted into four peaks (Fig. 2D). The peaks were observed at 286.18, 286.98, 288.88, and 294.78 eV belong to C-C bond [50], C-N/C-O or C=O bonds [45], amide groups (N-C=O) [51], and π - π^* interaction [52].

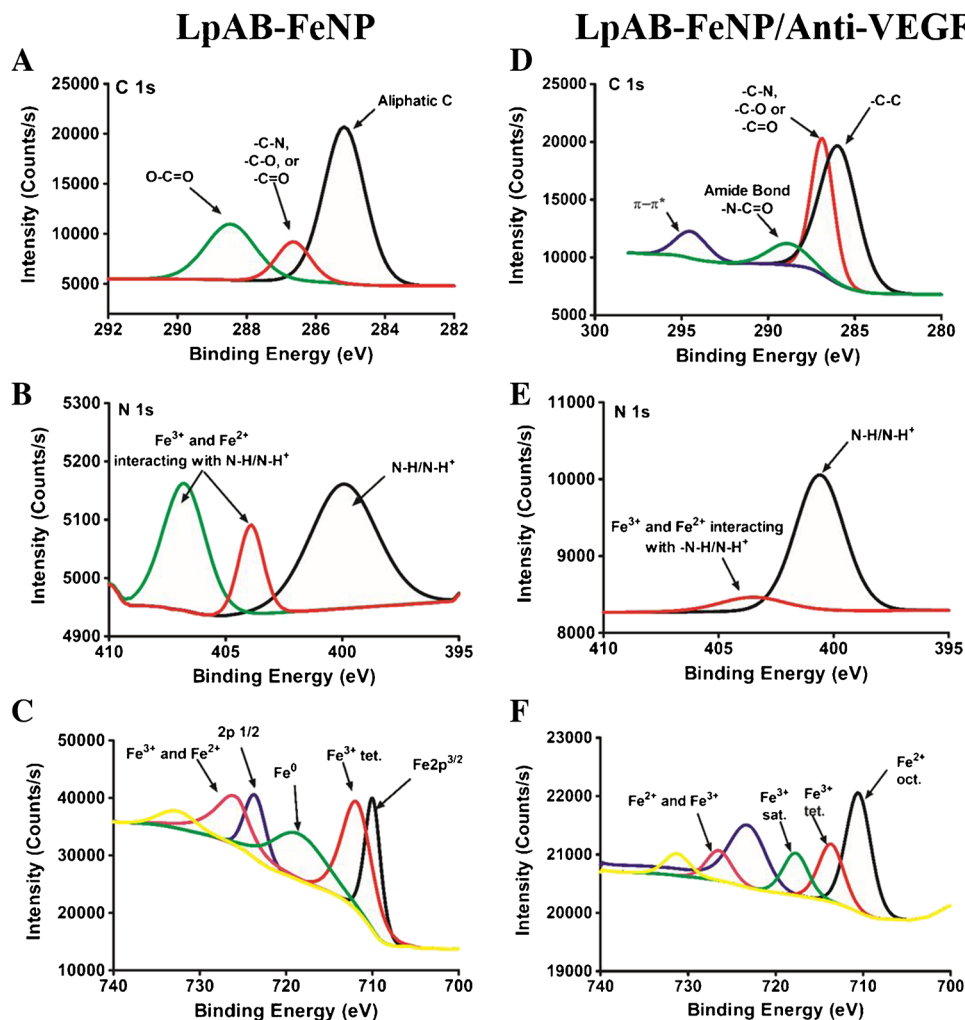
Figure 2B shows the N 1 s spectrum, which exhibited three peaks corresponding to N-H/N-H+ [53], Fe^{2+} , and Fe^{3+} interacting N-H/N-H+ at 399.98, 403.98, and 406.88 eV, respectively [54]. The N 1 s deconvolution of LpAB-FeNP/anti-VEGF (Fig. 2E) gave two distinct groups of peaks. The peaks at 400.68 and 403.78 eV correspond to N-H, N-H+, N-O [55], and amide groups (N-C=O) [56],

respectively, which support the covalent linkage between LpAB-FeNP and anti-VEGF. In Fig. 2C and Fig. 2E, the characteristic peak of Fe 2p_{3/2} is expected at 710.2 eV, which is indicative of the core level spectra of Fe_3O_4 nanoparticles [57]. As illustrated, the peaks in the Fe 2p spectrum are situated at 726.68 eV for LpAB-FeNP and 710.88 eV for bivalent iron (Fe^{2+}) in LpAB-FeNP/anti-VEGF. Furthermore, the peaks at 712.48, 714.08, 718.38, and 726.98 eV can be attributed to trivalent iron (Fe^{3+}) [58]. The component at 724.08 eV corresponds to Fe 2p_{1/2}. According to the literature, the characteristic peak of zerovalent Fe (Fe^0) is expected at 719.9 eV [56]. As shown in Fig. 2F, a characteristic peak at 719.98 eV for Fe^0 is observed. Combining all the XPS results, it can be concluded that the anti-VEGF has been successfully conjugated onto the surface of LpAB-FeNP.

Analytical characterization of VEGF LpAB-FeNP/anti-VEGF

Enzyme-mimicking nanomaterials have emerged as potential substitutes for natural proteins [59]. Similarly, an antibody-based immunoassay was developed for C-reactive protein (CRP) [45] where a metal organic framework (MOF) labeled with anti-CRP was used as a probe. In the presence of CRP, the labeled anti-CRP forms a connection via affinity, and a fluorescence signal is generated depending on the target. In this study, a colorimetric analysis of immunoassay targeting different levels of VEGF_{165} was performed using colorimetric detection in PBS buffer (pH 7.4). Here, the LpAB-FeNP/anti-VEGF conjugate was employed as the detection antibody, which was captured by VEGF_{165} coated onto a 96-well plate. LpAB-FeNP served as the source of the colorimetric signal. The schematic presentation of the proposed immunoassay is given in Fig. 3.

Fig. 2 XPS spectrum of LpAB-FeNP. **A** C 1s LpAB-FeNP. **B** N 1s LpAB-FeNP. **C** Fe LpAB-FeNP. **D** C 1s LpAB-FeNP/anti-VEGF. **E** N 1s LpAB-FeNP/anti-VEGF. **F** Fe LpAB-FeNP/anti-VEGF



The investigated assay parameters for the detection were the concentration of BSA, VEGF₁₆₅ incubation time, and the concentration of anti-VEGF. The BSA concentration and incubation time for VEGF₁₆₅ were determined based on previous studies [45, 60]. The calibration curve of the proposed VEGF₁₆₅ determination assay exhibited a wide linear range between 0.5 and 100 ng/mL with the best fit equation of $y = 0.174x - 0.322$. Absorbance values of VEGF₁₆₅ Log (pg/mL) at different concentrations are shown in the Supplementary Materials file (Table S1). Additionally, the correlation coefficient (R^2) was calculated as 0.996, indicating a reliable relationship, as shown in Fig. 4B. Figure 4D presents an image depicting the potential impact of interferences on the proposed immunoassay platform.

The limit of detection (LOD) is a crucial parameter for assessing the analytical performance of a method with a certain level of confidence [61]. In the LpAB-FeNP/anti-VEGF immunoassay, the LOD was determined using 10 measurements at the lowest concentration (0.5 ng/mL) on the calibration curve. LOD was calculated using the formula $3SD/m$, where SD represents the standard deviation of 10 measurements performed at the lowest VEGF₁₆₅ concentration and

m represents the slope of the VEGF₁₆₅ calibration curve. The experimental determination of LOD in this study was 0.29 ng/mL.

Table 1 provides an overview of the comparison of some VEGF sensors described in the literature. Based on signal transducer types, immunoassays can be classified as electrochemical, colorimetric, or optical immunoassays. Among these, colorimetric immunoassays for disease biomarker detection have drawn much interest because of their ease of use and high level of effectiveness [62].

In the current literature, the tests are mostly performed using electrochemical and colorimetric methods. They frequently employ aptamer/antibody combinations, offering high specificity and selectivity. Furthermore, the repeatability, stability, and affordability of the test system can be improved by using antibodies and/or aptamers [75]. In our case, the results show that the prepared LpAB-FeNP/anti-VEGF has many advantages over the others, including a better LOD and a broader linear detection range. The repeatability of the immunoassay played a key role in our VEGF₁₆₅ measurement platform. We investigated the repeatability

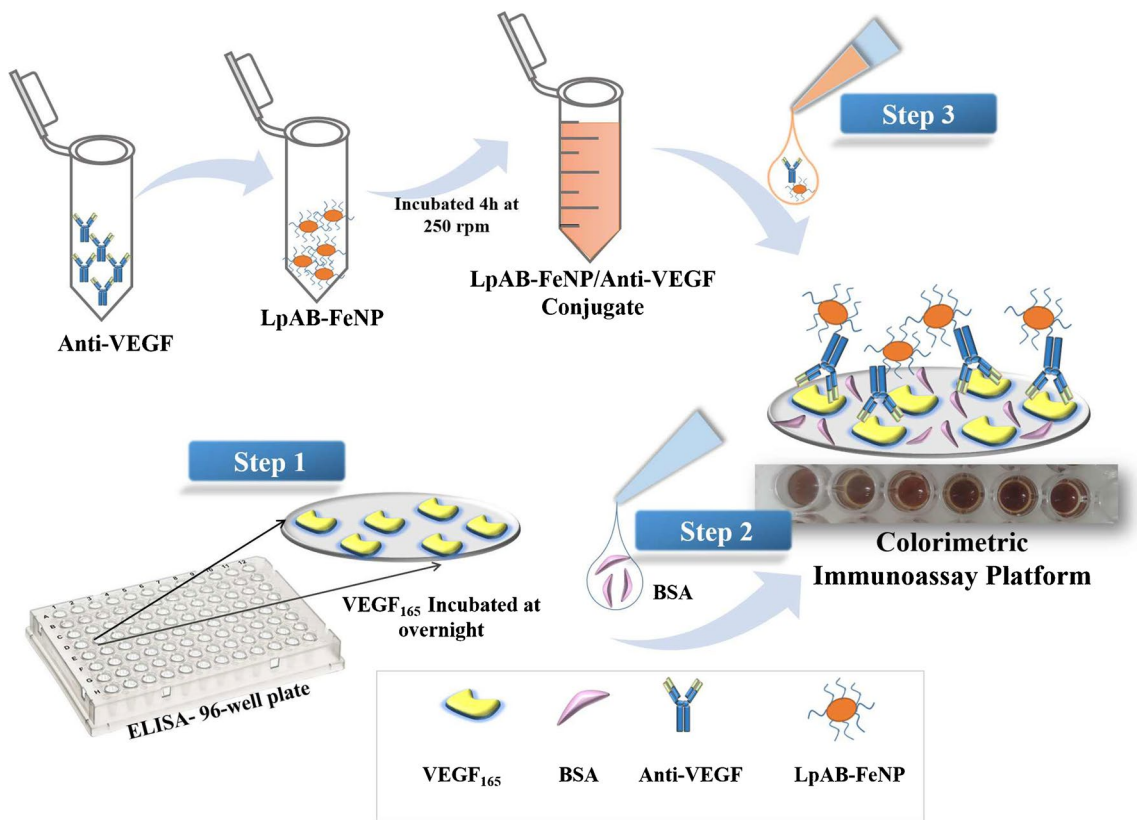
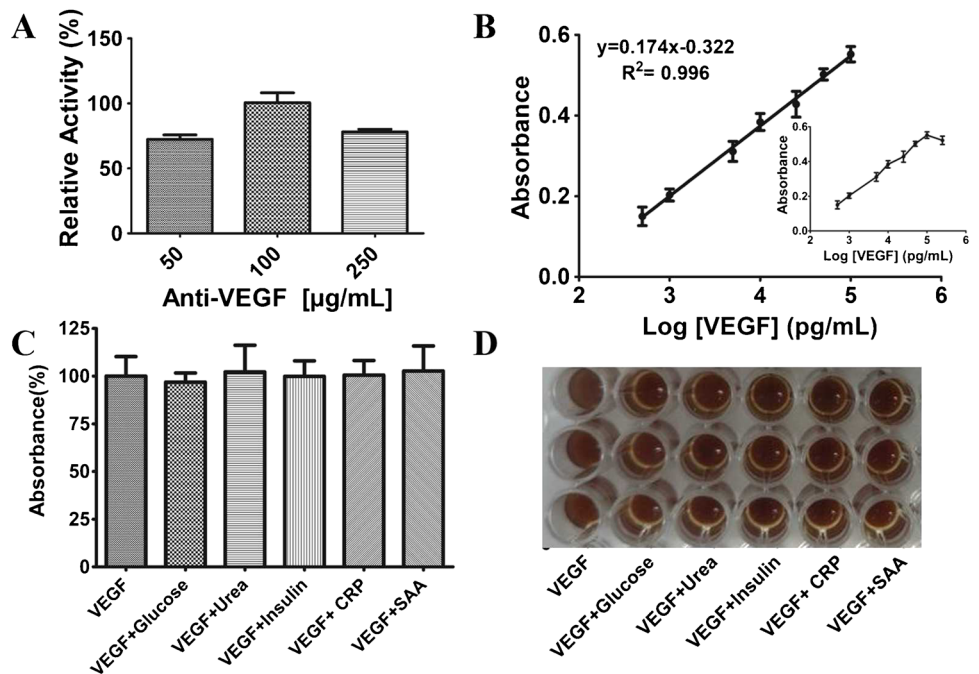


Fig. 3 Schematic demonstration of colorimetric immunoassay preparation platform

Fig. 4 **A** Optimization of anti-VEGF concentration. **B** Calibration curve of log VEGF₁₆₅ (pg/mL) constructed by linear fitting. **C** The result of the proposed FeNP-based ELISA assay for VEGF₁₆₅ detection over some potentially interfering substances: VEGF₁₆₅, 10 ng/mL; glucose, 10 mM; urea, 0.1 mg/mL; insulin, 10 μU/mL; CRP, 10 ng/mL; SAA, 10 ng/mL. **D** Representative example of interference results obtained in the ELISA plate. Error bars show SD of at least three measurements



through conducting eight measurements in the presence of 10 ng/mL VEGF₁₆₅ protein. The coefficient of variation (CV) of the platform was calculated as 0.152%.

The potential interference effects of glucose, urea, insulin, CRP, and SAA (common biological components found in blood) on the immunoassay response for detecting VEGF₁₆₅

Table 1 Comparison of VEGF determination studies summarized in literature

Target	Detection method	Nanomaterial	Linear detection for VEGF	LOD	Ref
VEGF	Electrochemical	RGO/Au NPs	2–20,000 ng/mL	6 fg/mL	[63]
VEGF	Fluorescence	GO/Aptamer	0.32–5.0 nM	0.32 nM	[64]
VEGF	Fluorescence	Quantum dot microspheres	25–1600 pg/mL	-	[65]
VEGF	Electrochemical	DNA aptamer	5 pM	50 pM–0.15 nM	[66]
VEGF	Electrochemical	GO/MB-AuNPs-aptamer-Fc sensing	2–500 pg/mL	0.1 pg/mL	[67]
VEGF	Electrochemical	AuNA@NC	0.01–10 ng/mL	6.77 pg/mL	[68]
VEGF ₁₆₅	Electrochemical	Fe ₃ O ₄ /Fe ₂ O ₃ @Au	0.01–10 pg/mL	0.01 pg/mL	[69]
VEGFR1	Electrochemical	Au/3-MPA	10–70 pg/mL	-	[70]
VEGF	Electrochemical	GO-ssDNA	0.05–100 ng/mL	50 pg/mL	[71]
VEGF	Electrochemical	Cd(II)@LP and Cu(II)@LP	0.01–7000 pg mL	0.005 pg/ mL	[72]
VEGF	Chemiluminescence	CdTe QD/H ₂ O ₂	2–35,000 pg/mL	0.5 pg/mL	[73]
VEGF ₁₆₅	Colorimetric	G-quadruplex DNAzymes/Cat	24.00 pM–11.25 nM	1.70 pM	[74]
VEGF ₁₆₅	Colorimetric	LpAB-FeNP	0.5–100 ng/mL	0.29 ng/mL	This study

RGO/Au NPs reduced graphene oxide/Au nanoparticles, *GO* G-quadruplex aptamer, *GO/MB-AuNPs-aptamer-Fc* graphene oxide/methylene blue-AuNP-ferrocene-labeled aptamer, *AuNA@NC* Au nanoarchitecture (Au NA) embedded with nanochitosan, *Fe₃O₄/Fe₂O₃@Au* magnetic iron-gold nanoparticles, *VEGFR1* vascular endothelial growth factor receptor-1, *Au/3-MPA* gold electrode/3-mercaptopropionic acid, *GO-ssDNA* graphene oxide/ssDNA, *Cd(II)@LP* cadmium-loaded liposome, *Cu(II)@LP* copper-loaded liposome, *Cat* catalase

were examined. The reference levels for the interferences are 0.35–5.0 mM for glucose [76], 0.10–0.16 mg/mL for urea [77], 2–20 mIU/mL for insulin [78], lower than 0.3 to 1.0 mg/mL in healthy individuals for CRP [79], and 0.02–0.05 mg/mL for SAA under normal conditions [80] according to literature. LpAB-FeNP/anti-VEGF/VEGF₁₆₅ was prepared, and the effect of each substance in the immunoassay response was evaluated using the colorimetric method in the presence of 10 ng/mL VEGF₁₆₅ (Fig. 4C, D). The selectivity was calculated to be 96.84% for VEGF₁₆₅ + glucose, 102.22% for VEGF₁₆₅ + urea, 99.86% for VEGF₁₆₅ + insulin, 100.54% for VEGF₁₆₅ + CRP, and 102.67% VEGF₁₆₅ + SAA as seen in Fig. 4C. The impact of the potential interferences was found to be lower than 5%, indicating that the immunoassay exhibited excellent selectivity. Therefore, glucose, urea, insulin, CRP, and SAA did not interfere with the LpAB-FeNP/anti-VEGF immunoassay platform.

The proposed immunosensor platform was employed to determine VEGF₁₆₅ in the artificial blood sample. A known amount of VEGF₁₆₅ (10 ng/mL) was added to artificial serum and determined the recovery % with LpAB-FeNP/anti-VEGF. The recovery % of VEGF₁₆₅ detection was calculated as 95.16%, and the relative standard deviation (RSS) was calculated as 5.08. Confirming the system's validity, the obtained result falls within the acceptable recovery range of 95–105% [81].

Conclusion

In this study, we successfully designed a colorimetric measurement system for the detection of VEGF₁₆₅. The developed LpAB-FeNP/anti-VEGF immunoassay platform

offers several advantages, including short analysis time, high accuracy, high specificity, reduced sample volume, and low cost. Besides, the wide linear range and low detection limit, this developed simple ELISA approach reduces the utilization of extended assay time and consumption of chemicals and antibodies. Therefore, the developed platform can be an alternative method in the detection of VEGF, which can be expanded to the detection of different analytes that are critically important in diagnostics.

Supplementary Information The online version contains supplementary material available at <https://doi.org/10.1007/s00604-024-06228-0>.

Acknowledgements The authors would like to thank Prof. Dr. Dilek Odacı in Biochemistry Department, Ege University, for the use of laboratory facilities and valuable comments.

Author contribution Conceptualization: Hülya Kuduğ Ceylan, Fatma Öztürk Kırbay, and İdris Yazgan; formal analysis and investigation: Hülya Kuduğ Ceylan, Fatma Öztürk Kırbay, and İdris Yazgan; writing—original draft preparation: Hülya Kuduğ Ceylan and Fatma Öztürk Kırbay; writing—review and editing: Hülya Kuduğ Ceylan, Fatma Öztürk Kırbay, İdris Yazgan, and Murat Elibol; funding acquisition: Murat Elibol; supervision: Murat Elibol and İdris Yazgan.

Funding Open access funding provided by the Scientific and Technological Research Council of Türkiye (TÜBİTAK). This study is supported by Ege University Scientific Research Projects Coordination Unit (Project Number FOA-2020–21791).

Data availability Data will be made available on request.

Declarations

Ethical approval This article does not contain any studies with human participants or animals performed by any of the authors.

Conflict of interest The authors declare no competing interests.

Open Access This article is licensed under a Creative Commons Attribution 4.0 International License, which permits use, sharing, adaptation, distribution and reproduction in any medium or format, as long as you give appropriate credit to the original author(s) and the source, provide a link to the Creative Commons licence, and indicate if changes were made. The images or other third party material in this article are included in the article's Creative Commons licence, unless indicated otherwise in a credit line to the material. If material is not included in the article's Creative Commons licence and your intended use is not permitted by statutory regulation or exceeds the permitted use, you will need to obtain permission directly from the copyright holder. To view a copy of this licence, visit <http://creativecommons.org/licenses/by/4.0/>.

References

- Shibuya M (2001) Structure and function of VEGF/VEGF-receptor system involved in angiogenesis. *Cell Struct Funct* 26:25–35. <https://doi.org/10.1247/csf.26.25>
- Shinkaruk S, Bayle M, Lañ G, Déléris G (2003) Vascular endothelial cell growth factor (VEGF), an emerging target for cancer chemotherapy. *Curr Med Chem Anticancer Agents* 3:95–117. <https://doi.org/10.2174/1568011033353452>
- Carmeliet P, Jain RK (2011) Molecular mechanisms and clinical applications of angiogenesis. *Nature* 473:298. <https://doi.org/10.1038/NATURE10144>
- Olsson AK, Dimberg A, Kreuger J, Claesson-Welsh L (2006) VEGF receptor signaling? In control of vascular function. *Nat Rev Mol Cell Biol* 7:359–371. <https://doi.org/10.1038/nrm1911>
- Shibuya MJB (2013) Vascular endothelial growth factor and its receptor system: physiological functions in angiogenesis and pathological roles in various diseases. *J Biochem* 153(1):13–19. <https://doi.org/10.1093/jb/mvs136>
- Bao P, Kodra A, Tomic-Canic M, Golinko MS, Ehrlich H, Brem H (2009) The role of vascular endothelial growth factor in wound healing. *J Surg Res* 153:347–358. <https://doi.org/10.1016/J.JSS.2008.04.023>
- Dong Q, Cheng Z (2003) Functions of VEGF in female reproductive system. *Chin Sci Bull* 48:217–222. <https://doi.org/10.1007/bf03183286>
- Haigh JJ (2008) Role of VEGF in organogenesis. *Organogenesis* 4(4):247–256. <https://doi.org/10.4161/org.4.4.7415>
- Gu C, Rodriguez ER, Reimert DV, Shu T, Fritsch B, Richards LJ, Kolodkin AL, Ginty DD (2003) Neuropilin-1 conveys semaphorin and VEGF signaling during neural and cardiovascular development. *Dev Cell* 5(1):45–57. [https://doi.org/10.1016/S1534-5807\(03\)00169-2](https://doi.org/10.1016/S1534-5807(03)00169-2)
- Chen Q, Wang Z, Yang C, Li B, Ren X, Liu C, Xi L (2023) High resolution intravital photoacoustic microscopy reveals VEGF-induced bone regeneration in mouse tibia. *Bone* 167:116631. <https://doi.org/10.1016/j.bone.2022.116631>
- Gerber HP, Ferrara N (2003) The role of VEGF in normal and neoplastic hematopoiesis. *J Mol Med* 81(1):20–31. <https://doi.org/10.1007/s00109-002-0397-4>
- Malemud CJ (2007) Growth hormone, VEGF and FGF: involvement in rheumatoid arthritis. *Clin Chim Acta* 375:10–19. <https://doi.org/10.1016/J.CCA.2006.06.033>
- Xiong N, Zhang Z, Huang J, Chen C, Zhang Z, Jia M, Xiong J, Liu X, Wang F, Cao X, Liang Z, Sun S, Lin Z, Wang T (2011) VEGF-expressing human umbilical cord mesenchymal stem cells, an improved therapy strategy for Parkinson's disease. *Gene Ther* 18:394–402. <https://doi.org/10.1038/gt.2010.152>
- Canavese M, Altruda F, Ruzicka T, Schaubert J (2010) Vascular endothelial growth factor (VEGF) in the pathogenesis of psoriasis—a possible target for novel therapies? *J Dermatol Sci* 58:171–176. <https://doi.org/10.1016/J.JDERMMSCI.2010.03.023>
- Nichani PAH, Popovic MM, Dhoot AS, Pathak A, Muni RH, Kertes PJ (2023) Treat-and-extend dosing of intravitreal anti-VEGF agents in neovascular age-related macular degeneration: a meta-analysis. *Eye (Lond)* 37(14):2855–2863. <https://doi.org/10.1038/s41433-023-02439-6>
- Gupta N, Mansoor S, Sharma A, Sapkal A, Sheth J, Falatoonzadeh P, Kuppermann B, Kenney M (2013) Diabetic retinopathy and VEGF. *Open Ophthalmol J* 7:4–10. <https://doi.org/10.2174/1874364101307010004>
- Ferrara N (2000) VEGF: an update on biological and therapeutic aspects. *Curr Opin Biotechnol* 11(6):617–624. [https://doi.org/10.1016/s0958-1669\(00\)00153-1](https://doi.org/10.1016/s0958-1669(00)00153-1)
- Yang Y, Cao Y (2022) The impact of VEGF on cancer metastasis and systemic disease. *Semin Cancer Biol* 86:251–261. <https://doi.org/10.1016/j.semcancer.2022.03.011>
- Wahyuni E, Hariman H, Edianto D (2021) Relationship between plasma vascular endothelial growth factor (VEGF) and ovarian cancer staging. *Int J Res Rev* 8:7. <https://doi.org/10.52403/ijrr.20210714>
- Costache MI, Ioana M, Iordache S, Ene D, Costache CA, Săftoiu A (2015) VEGF expression in pancreatic cancer and other malignancies: a review of the literature. *Rom J Intern Med* 53(3):199–208. <https://doi.org/10.1515/rjim-2015-0027>
- Kim MS, Park TI, Lee YM, Jo YM, Kim S (2013) Expression of Id-1 and VEGF in non-small cell lung cancer. *Int J Clin Exp Pathol* 6(10):2102–2111
- Divya JDI, Prathipaa RPR, Keerthini GKG (2022) Expression of VEGF in breast cancer. *Int J Health Sci* 6(S7):6396–6400. <https://doi.org/10.53730/ijhs.v6nS7.13532>
- Lin X, Khalid S, Qureshi MZ, Attar R, Yaylim I, Ucak I, Yaqub A, Fayyaz S, Farooqi AA, Ismail M (2016) VEGF mediated signaling in oral cancer. *Cell Mol Biol* 62(14):64–68
- Mohamed SY, Mohammed HL, Ibrahim HM, Mohamed EM, Salah M (2019) Role of VEGF, CD105, and CD31 in the prognosis of colorectal cancer cases. *J Gastrointest Cancer* 50(1):23–34. <https://doi.org/10.1007/s12029-017-0014-y>
- Dong G, Lin XH, Liu HH, Gao DM, Cui JF, Ren ZG, Chen RX (2019) Intermittent hypoxia alleviates increased VEGF and pro-angiogenic potential in liver cancer cells. *Oncol Lett* 18(2):1831–1839. <https://doi.org/10.3892/ol.2019.10486>
- Cabral T, Lima LH, Polido J, Duong J, Okuda É, Oshima A, Serracarbassa P, Regatieri CV, Belfort R Jr (2017) Aqueous vascular endothelial growth factor and clinical outcomes correlation after single intravitreal injection of bevacizumab in patients with neovascular age-related macular degeneration. *Int J Retina Vitreous* 3:6. <https://doi.org/10.1186/s40942-017-0066-y>
- Dehghani S, Nosrati R, Yousefi M, Nezami A, Soltani F, Taghdisi SM, Abnous K, Alibolandi M, Ramezani M (2018) Aptamer-based biosensors and nanosensors for the detection of vascular endothelial growth factor (VEGF): a review. *Biosens Bioelectron* 1(110):23–37. <https://doi.org/10.1016/j.bios.2018.03.037>
- Vernes JM, Gloria Meng Y (2015) Detection and quantification of VEGF isoforms by ELISA. *Methods in Mol Biol* 1332:25–37. https://doi.org/10.1007/978-1-4939-2917-7_2
- Li L, Li M, Pang Y, Wang J, Wan Y, Zhu C, Yin Z (2019) Abnormal thyroid hormone receptor signaling in osteoarthritic osteoblasts regulates microangiogenesis in subchondral bone. *Life Sci* 239:116975. <https://doi.org/10.1016/j.lfs.2019.116975>

30. Anderson SM, Chen TT, Iruela-Arispe ML, Segura T (2009) The phosphorylation of vascular endothelial growth factor receptor-2 (VEGFR-2) by engineered surfaces with electrostatically or covalently immobilized VEGF. *Biomaterials* 30:4618–4628. <https://doi.org/10.1016/j.biomaterials.2009.05.030>
31. Suzuki Y, Yokohama K (2009) Development of a fluorescent peptide for the detection of vascular endothelial growth factor (VEGF). *Chem Bio Chem* 10:1793–1795. <https://doi.org/10.1002/CBIC.200900190>
32. Fu XM, Liu ZJ, Cai SX, Zhao YP, Wu DZ, Li CY, Chen JH (2016) Electrochemical aptasensor for the detection of vascular endothelial growth factor (VEGF) based on DNA-templated Ag/Pt bimetallic nanoclusters. *Chin Chem Lett* 27:920–926. <https://doi.org/10.1016/J.CCLET.2016.04.014>
33. Li W, Zhang Q, Zhou H, Chen J, Li Y, Zhang C, Yu C (2015) Chemiluminescence detection of a protein through the aptamer-controlled catalysis of a porphyrin probe. *Anal Chem* 87(16):8336–8341. <https://doi.org/10.1021/acs.analchem.5b01511>
34. Billingsley MM, Riley RS, Day ES (2017) Antibody-nanoparticle conjugates to enhance the sensitivity of ELISA-based detection methods. *PLoS ONE* 12(5):e0177592. <https://doi.org/10.1371/journal.pone.0177592>
35. Xu N, Jin S, Wang L (2021) Metal nanoparticles-based nano-platforms for colorimetric sensing: a review. *Rev Anal Chem* 40(1):1–11. <https://doi.org/10.1515/revac-2021-0122>
36. Zhu X, Kou F, Xu H, Lin L, Yang G, Lin Z (2017) A highly sensitive aptamer-immunoassay for vascular endothelial growth factor coupled with portable glucose meter and hybridization chain reaction. *Sens Actuators B Chem* 253:660–665. <https://doi.org/10.1016/J.SNB.2017.06.174>
37. Jazayeri MH, Amani H, Pourfatollah AA, Pazoki-Toroudi H, Sedighimoghaddam B (2016) Various methods of gold nanoparticles (GNPs) conjugation to antibodies. *Sens Biosensing Res* 9:17–22. <https://doi.org/10.1016/j.sbsr.2016.04.002>
38. KuduğCeylan H, ErdenTayhan S, Gökçe İ (2021) Secretory expression of human vascular endothelial growth factor (VEGF165) in *Kluyveromyces lactis* and characterization of its biological activity. *Int J Pept Res Ther* 27:1989–2001. <https://doi.org/10.1007/s10989-021-10227-7>
39. Gal JY, Fovet Y, Adib-Yadzi M (2001) About a synthetic saliva for in vitro studies. *Talanta* 53:1103–1115. [https://doi.org/10.1016/s0039-9140\(00\)00618-4](https://doi.org/10.1016/s0039-9140(00)00618-4)
40. Li L, Mak KY, Leung CW, Chan KY, Zhong W, Pong PWT (2013) Effect of synthesis conditions on the properties of citric-acid coated iron oxide nanoparticles. *Microelectron Eng* 110:329–334. <https://doi.org/10.1016/j.mee.2013.02.045>
41. Saraswathy A, Nazeer SS, Jeevan M, Nimi N, Arumugam S, Harikrishnan VS, Varma PR, Jayasree RS (2014) Citrate coated iron oxide nanoparticles with enhanced relaxivity for in vivo magnetic resonance imaging of liver fibrosis. *Colloids Surf B Biointerfaces* 117:216–224. <https://doi.org/10.1016/j.colsurfb.2014.02.034>
42. Yazgan I, Gümüş A, Gökkuş K, Demir MA, Evecen S, Sönmez HA, Miller RM, Bakar F, Oral A, Popov S, Toprak MS (2020) On the effect of modified carbohydrates on the size and shape of gold and silver nanostructures. *Nanomaterials* 10:1–17. <https://doi.org/10.3390/nano10071417>
43. Saladino GM, Hamawandi B, Demir MA, Yazgan I, Toprak MS (2021) A versatile strategy to synthesize sugar ligand coated superparamagnetic iron oxide nanoparticles and investigation of their antibacterial activity. *Colloids Surf A Physicochem Eng Asp* 613:126086. <https://doi.org/10.1016/j.colsurfa.2020.126086>
44. Hermanson GT (2013) *Bioconjugate techniques*, 3rd edn. Academic Press, Boston
45. Kirbay FO, Yazgan İ, Demirkol DO (2022) Comparison of direct and sandwich type immunoassays on electrospun nanofibers using of metal organic frameworks as a fluorescence probe. *Sens Actuators B Chem* 372:132621. <https://doi.org/10.1016/j.snb.2022.132621>
46. Padilla-Cruz AL, Garza-Cervantes JA, Vasto-Anzaldo XG, García-Rivas G, León-Buitimea A, Morones-Ramírez JR (2021) Synthesis and design of Ag–Fe bimetallic nanoparticles as antimicrobial synergistic combination therapies against clinically relevant pathogens. *Sci Rep* 11(1):5351. <https://doi.org/10.1038/s41598-021-84768-8>
47. Bikkarolla SK, McNamee SE, McGregor S, Vance P, EL McGhee H M, McLaughlin J (2020) A lateral flow immunoassay with self-sufficient microfluidic system for enhanced detection of thyroid-stimulating hormone. *AIP Adv* 10(12):125316. <https://doi.org/10.1063/5.0026047>
48. Yazgan I, Osonga FJ, Miller RM, Kariuki VM, Zhang J, Feng J, Skeete Z, Crapo H, Schulte J SOA (2021) Greener one-pot synthesis of gold nanoparticle glycoconjugates using functionalized sugars. *ACS Agric Sci Technol* 1(4):379–389. <https://doi.org/10.1021/acscagtech.1c00093>
49. Noval VE, Carriazo JG (2019) Fe₃O₄-TiO₂ and Fe₃O₄-SiO₂ core-shell powders synthesized from industrially processed magnetite (Fe₃O₄) microparticles. *Mater Res* 22(3):e20180660. <https://doi.org/10.1590/1980-5373-MR-2018-0660>
50. Wu Z, Wang L (2019) Graphene oxide (GO) doping hexagonal flower-like ZnO as potential enhancer of photocatalytic ability. *Mater Lett* 234:287–290. <https://doi.org/10.1016/j.matlet.2018.09.128>
51. Kehrer M, Duchoslav J, Hinterreiter A, Cobet M, Mehic A, Stehrer T, Stifter D (2019) XPS investigation on the reactivity of surface imine groups with TFAA. *Plasma Process Polym* 16:e1800160. <https://doi.org/10.1002/ppap.201800160>
52. Tawil N, Sacher E, Boulais E, Mandeville R, Meunier M (2013) X-ray photoelectron spectroscopic and transmission electron microscopic characterizations of bacteriophage-nanoparticle complexes for pathogen detection. *J Phys Chem C* 117(40):20656–20665. <https://doi.org/10.1021/jp406148h>
53. Šetka M, Calavia R, Vojtkůvka L, Llobet E, Drbohlavová J, Vallejos S (2019) Raman and XPS studies of ammonia sensitive polypyrrole nanorods and nanoparticles. *Sci Rep* 9:8465. <https://doi.org/10.1038/s41598-019-44900-1>
54. Men S, Mitchell DS, Lovelock KRJ, Licence P (2015) X-ray photoelectron spectroscopy of pyridinium-based ionic liquids: comparison to imidazolium- and pyrrolidinium-based analogues. *ChemPhysChem* 16(10):2211–2218. <https://doi.org/10.1002/cphc.201500227>
55. Hamid HS, Eric F (2006) XPS & FTIR Study of adsorption characteristics using cationic and anionic collectors on smithsonite. *J Miner Mater Char Eng* 5(1):21–45. <https://doi.org/10.4236/jmmce.2006.51002>
56. Rosenberger L, Baird R, McCullen E, Auner G, Shreve G (2008) XPS analysis of aluminum nitride films deposited by plasma source molecular beam epitaxy. *Surf Interface Anal* 40:1254–1261. <https://doi.org/10.1002/sia.2874>
57. Singh N, Nayak J, Sahoo SK, Kumar R (2019) Glutathione conjugated superparamagnetic Fe₃O₄-Au core shell nanoparticles for pH-controlled release of DOX. *Mater Sci Eng C* 100:453–465. <https://doi.org/10.1016/j.msec.2019.03.031>
58. Li P, Xuan Y, Jiang B, Zhang S, Xia C (2022) Hollow La_{0.6}Sr_{0.4}Ni_{0.2}Fe_{0.75}Mo_{0.05}O_{3-δ} electrodes with exsolved FeNi₃ in quasi-symmetrical solid oxide electrolysis cells for direct CO₂ electrolysis. *Electrochem Commun* 134:107188. <https://doi.org/10.1016/j.elecom.2021.107188>
59. Xia Y, Liu M, Wang L, Yan A, He W, Chen M, Lan J, Xu J, Guan L, Chen J (2017) A visible and colorimetric aptasensor based

- on DNA-capped single-walled carbon nanotubes for detection of exosomes. *Biosens Bioelectron* 92:8–15. <https://doi.org/10.1016/j.bios.2017.01.063>
60. Singh AK, Yadav S, Chauhan BS, Nandy N, Singh R, Neogi K, Roy JK, Srikrishna S, Singh RK, Prakash P (2019) Classification of clinical isolates of *Klebsiella pneumoniae* based on their in vitro biofilm forming capabilities and elucidation of the biofilm matrix chemistry with special reference to the protein content. *Front Microbiol* 4(10):669. <https://doi.org/10.3389/fmicb.2019.00669>
 61. Vashist SK, Luong JHT (2018) Bioanalytical requirements and regulatory guidelines for immunoassays. In: *Handbook of Immunoassay Technologies*. Academic Press, pp 81–95
 62. Liu L, Hao Y, Deng D, Xia N (2019) Nanomaterials-based colorimetric immunoassays. *Nanomaterials* 9(3):316. <https://doi.org/10.3390/nano9030316>
 63. Pourmadadi M, Shayeh JS, Arjmand S, Omid M, Fatemi F (2020) An electrochemical sandwich immunosensor of vascular endothelial growth factor based on reduced graphene oxide/gold nanoparticle composites. *Microchem J* 159:105476. <https://doi.org/10.1016/j.microc.2020.105476>
 64. Park Y, Hong MS, Lee WH, Kim JG, Kim K (2021) Highly sensitive electrochemical aptasensor for detecting the VEGF165 tumor marker with pani/cnt nanocomposites. *Biosensors (Basel)* 11:1–11. <https://doi.org/10.3390/bios11040114>
 65. Wang S, Lu H, Wang L, Zou J, Zhang R (2020) Rapid determination of serum vascular endothelial growth factor (VEGF) by a fluorescence immunochromatographic assay. *Anal Lett* 54:1233–1241. <https://doi.org/10.1080/00032719.2020.1798455>
 66. Zhao S, Yang W, Lai RY (2011) A folding-based electrochemical aptasensor for detection of vascular endothelial growth factor in human whole blood. *Biosens Bioelectron* 26:2442–2447. <https://doi.org/10.1016/j.bios.2010.10.029>
 67. Ni S, Shen Z, Zhang P, Liu G (2020) Enhanced performance of an electrochemical aptasensor for real-time detection of vascular endothelial growth factor (VEGF) by nanofabrication and ratiometric measurement. *Anal Chim Acta* 1121:74–82. <https://doi.org/10.1016/J.ACA.2020.05.003>
 68. Wang H, Ma Y, Guo C, Yang Y, Peng Z, Liu Z, Zhang Z (2019) Templated seed-mediated derived Au nanoarchitectures embedded with nanochitosan: sensitive electrochemical aptasensor for vascular endothelial growth factor and living MCF-7 cell detection. *Appl Surf Sci* 481:505–514. <https://doi.org/10.1016/J.APSUSC.2019.03.148>
 69. Zhang Y, Liu M, Pan S, Li Yu, Zhang S, Liu R (2022) A magnetically induced self-assembled and label-free electrochemical aptasensor based on magnetic Fe₃O₄/Fe₂O₃@Au nanoparticles for VEGF₁₆₅ protein detection. *Appl Surf Sci* 580:152362. <https://doi.org/10.1016/j.apsusc.2021.152362>
 70. Sezgintürk MK (2011) A new impedimetric biosensor utilizing VEGF receptor-1 (Flt-1): early diagnosis of vascular endothelial growth factor in breast cancer. *Biosens Bioelectron* 26:4032–4039. <https://doi.org/10.1016/j.bios.2011.03.025>
 71. Pan LH, Kuo SH, Lin TY, Lin CW, Fang PY, Yang HW (2017) An electrochemical biosensor to simultaneously detect VEGF and PSA for early prostate cancer diagnosis based on graphene oxide/ssDNA/PLLA nanoparticles. *Biosens Bioelectron* 89:598–605. <https://doi.org/10.1016/j.bios.2016.01.077>
 72. Johari-Ahar M, Karami P, Ghanei M, Afkhami A, Bagheri H (2018) Development of a molecularly imprinted polymer tailored on disposable screen-printed electrodes for dual detection of EGFR and VEGF using nano-liposomal amplification strategy. *Biosens Bioelectron* 107:26–33. <https://doi.org/10.1016/j.bios.2018.02.005>
 73. Ghavamipour F, Rahmani H, Shanehsaz M, Khajeh K, Mirshahi M, Sajedi RH (2020) Enhanced sensitivity of VEGF detection using catalase-mediated chemiluminescence immunoassay based on CdTe QD/H₂O₂ system. *J Nanobiotechnology* 18:1–10. <https://doi.org/10.1186/s12951-020-00648-9>
 74. Zhang H, Peng L, Li M, Ma J, Qi S, Chen H, Zhou L, Chen X (2017) A label-free colorimetric biosensor for sensitive detection of vascular endothelial growth factor-165. *Analyst* 142:2419–2425. <https://doi.org/10.1039/c7an00541e>
 75. Davydova A, Vorobyeva M (2022) Aptamer-based biosensors for the colorimetric detection of blood biomarkers: paving the way to clinical laboratory testing. *Biomedicines* 10(7):1606. <https://doi.org/10.3390/biomedicines10071606>
 76. Ginsberg BH (2009) Factors affecting blood glucose monitoring: Sources of errors in measurement. *J Diabetes Sci Technol* 3(4):903–913. <https://doi.org/10.1177/193229680900300438>
 77. Guven G, Hilty MP, Ince C (2020) Microcirculation: physiology, pathophysiology, and clinical application. *Blood Purif* 49(1–2):143–150. <https://doi.org/10.1159/000503775>
 78. Chevenne D, Trivin F, Porquet D (1999) Insulin assays and reference values. *Diabetes Metab* 25(6):459–476
 79. Sproston NR, Ashworth JJ (2018) Role of C-reactive protein at sites of inflammation and infection. 9:1–11. <https://doi.org/10.3389/fimmu.2018.00754>
 80. Sack GH (2018) Serum amyloid A - a review. *Mol Med* 24:46. <https://doi.org/10.1186/s10020-018-0047-0>
 81. Taverniers I, De Loose M, Van Bockstaele E (2004) Trends in quality in the analytical laboratory. II. Analytical method validation and quality assurance. *TrAC Trends Anal Chem* 23:535–552. <https://doi.org/10.1016/j.trac.2004.04.001>

Publisher's Note Springer Nature remains neutral with regard to jurisdictional claims in published maps and institutional affiliations.